

## Microstructural Characterization of a Fe-25Mn-3Al-3Si TWIP–TRIP Steel

J T Benzing<sup>1</sup>, J Bentley<sup>2</sup>, W Poling<sup>3</sup>, K Findley<sup>3</sup>, D T Pierce<sup>4</sup>, J M Sosa<sup>5</sup>, H L Fraser<sup>5</sup>, D Raabe<sup>6</sup>, J E Wittig<sup>1</sup>

- <sup>1</sup>. Interdisciplinary Materials Science, Vanderbilt University, Nashville TN, USA
- <sup>2</sup>. Microscopy and Microanalytical Sciences, PO Box 7103, Oak Ridge, TN, USA
- <sup>3</sup>. Metallurgical and Materials Engineering, Colorado School of Mines, Golden, CO, USA
- <sup>4</sup>. Materials Science & Technology Division, Oak Ridge National Laboratory, Oak Ridge, TN, USA
- <sup>5</sup>. Materials Science and Engineering, The Ohio State University, Columbus, OH, USA
- <sup>6</sup>. Max-Planck-Institut für Eisenforschung, Max-Planck-Straße 1, Düsseldorf, Germany

This research utilizes electron backscattered diffraction (EBSD), electron channeling contrast imaging (ECCI) and conventional dark-field transmission electron microscopy (DF-TEM) to quantify the thickness and spacing of planar defects in a high-Mn steel. Fe-25Mn-3Al-3Si is considered a 2<sup>nd</sup> generation advanced high strength steel (AHSS) because the single-phase austenitic microstructure strain hardens via the TWIP and TRIP effects (twinning and transformation-induced plasticity). The secondary defects produced by TWIP/TRIP act as obstacles to subsequent dislocation motion in the microstructure, resulting in a high product of strength and elongation (PSE), which is attractive to the automotive industry for reduced weight, crashworthiness and cold stamping of complex parts [1]. The secondary planar defects which develop during deformation of the TWIP-TRIP alloy, (Figure 1a), include deformation twinning and  $\epsilon$ -martensite, both depending on a moderate stacking fault energy (SFE) of  $21 \pm 3$  mJ/m<sup>2</sup> [2,3]. The dynamic Hall-Petch effect is a result of continued refinement of the microstructure, but a more complete understanding involves the development of nucleation sites for deformation twinning and hexagonal  $\epsilon$ -martensite in relation to differing substructures and spacing [4]. Temperature and strain rate have opposing effects on mechanical properties of TWIP steels [5]. However, SFE is sensitive to temperature and governs the balance between the TWIP-TRIP phenomena. Current work utilizes servo-hydraulic tension across a range of strain rates (0.0002 – 200  $\epsilon$ /s), which can be interrupted so as to characterize the evolution in microstructure [6]. Load ringing in 200  $\epsilon$ /s tests is smoothed via a combination of a triple moving average and a spline fit to peak-valley midpoints. Each test also includes non-contact thermal imaging at 200 frames/s, allowing measurement of average temperature in the area of uniform elongation. Servo-hydraulic tensile tests show that increased strain rates result in a higher PSE and a significant rise in adiabatic heating within the area of uniform elongation, (Figure 1b-e).

In each interrupted sample, 3 mm diameter discs were electro discharge-machined (EDM) orthogonal to the gage sections, with a small protrusion left on the disc to indicate tensile direction. To achieve the necessary quality for proper EBSD and ECCI measurements, the 3 mm discs were mounted, ground by hand, auto-polished through 6, 3 & 1  $\mu$ m diamond suspensions, etched with 5% nitric acid in methanol to remove surface deformation, and auto-polished with 50 nm colloidal silica, ending in rinses with a soap-water mixture followed by ethanol. Micro-hardness indents were placed in a grid on the 3mm disc to act as markers during imaging and also to estimate Vickers hardness at a given interrupted strain. Figure 2a shows images recorded on different microscopes, such that EBSD is used to survey grains with  $\langle 101 \rangle$  orientations parallel to the beam direction, (recorded on a TESCAN Vega3LMU at 25 kV). Of those properly oriented grains, ECCI is used to first survey for proper channeling conditions, then a slow scan of the planar defects is recorded at high magnification on a Zeiss Merlin at 25kV. In the case of TEM sample preparation, discs were ground by hand and electropolished to electron transparency with a Struers twin-jet system (20% HNO<sub>3</sub>/80% CH<sub>3</sub>OH, -30 °C, 15 V). Proper DF-TEM diffracting conditions were achieved on an FEI Osiris at 200 kV by surveying grains with convergent beam electron diffraction (CBED) to find the  $\langle 101 \rangle$  orientation and then selecting the appropriate extra reflections (twinning or  $\epsilon$ -martensite) in selected area electron diffraction (SAED) with a sufficiently small (10  $\mu$ m) objective aperture to produce an unambiguous DF image (Figure 2b). Following the necessary recipe (FFT filter, adaptive threshold, black-white inversion, feature rejection and watershed) to segment planar defects from an image via MIPAR software [7], measurements of thickness and spacing of secondary deformation were made. Whereas DF-TEM provides excellent contrast and orientation information for the planar twin and  $\epsilon$ -martensite defects, EBSD and ECCI yield improved statistics for quantification. Preliminary measurements of one 3 mm disk per technique, (Figure 2c-d), with average spacing and thickness indicated by dotted lines, are based on the following sample distribution: DF-TEM (2 grains, 8 images) & ECCI (12 grains, 16 images). Additional measurements are underway with other tensile samples interrupted after  $\epsilon = 0.2$ , for various strain rates so as to quantify the effect of strain rate on microstructure [8].

References:

- [1] Y K Lee and J Han, *Mater. Sci. and Tech.*, **31-7** (2015), p. 843.
- [2] D T Pierce *et al*, *Acta Mater.*, **68** (2014), p. 238.
- [3] D T Pierce *et al*, *Acta Mater.*, **100** (2015), p. 178.
- [4] I Gutierrez-Urrutia and D Raabe, *Scripta Mater.*, **66** (2012), p. 992.
- [5] G T Gray III, *Annu. Rev. Mater. Res.*, **42** (2012), p. 285.
- [6] I Choi *et al*, *SAE World Con & Ex.*, **1434** (2006), p. 95.
- [7] J M Sosa *et al*, *Integr. Mater. Manuf. Innov.*, **3** (2014), p. 18.
- [8] This work was funded by the US National Science Foundation, Division of Materials Research under grant DMR1309258, NSF EPS 1004083, the MPIE in Düsseldorf, Germany and the Advanced Steel Processing and Products Research Center at Colorado School of Mines. Prof D G Walker provided the infra-red camera and Prof G Gualda and A Covey provided the EBSD measurements (all are at Vanderbilt University).

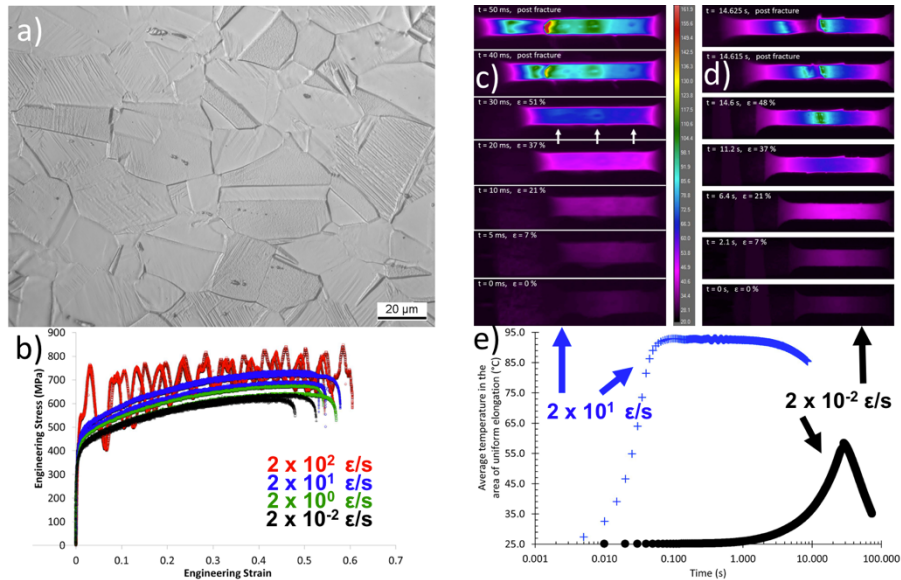


**Figure 1.** a) Light optical image of an etched microstructure after  $\epsilon = 0.2$ , pulled at  $20 \epsilon/s$ , b) mechanical data (before smoothing) acquired on a servo-hydraulic load frame, c-e) thermal imaging and the corresponding average temperature measured in the area of uniform elongation for indicated strain rates.

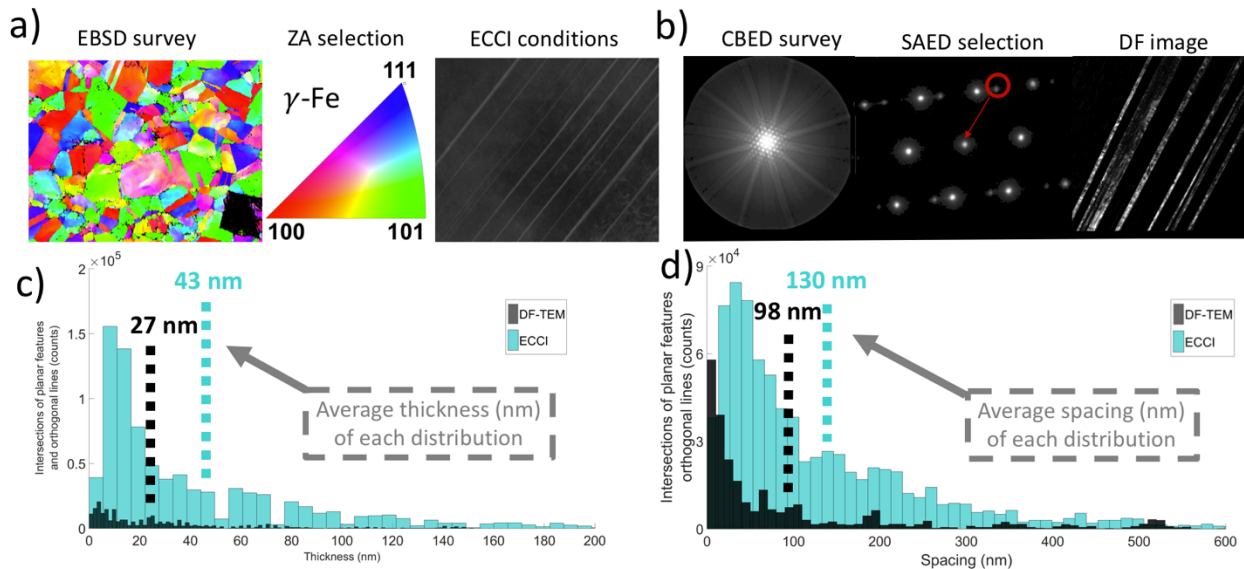


**Figure 2.** a) EBSD inverse pole figure map, orientation key and ECCI results of a BSE survey of the same area. b) Use of CBED survey and selection of twinning reflections in SAED to produce a DF-TEM image. c) thickness and d) spacing of planar defects measured from a sample pulled at  $20 \epsilon/s$ , interrupted at  $\epsilon = 0.2$ .